Dinaphthooxepine Bisimide Undergoes Oxygen Extrusion Reaction upon Electron Injection at Room Temperature

Mai Odajima,[†] Norihito Fukui,*[,†,‡] and Hiroshi Shinokubo*[,†]

† Department of Molecular and Macromolecular Chemistry, Graduate School of Engineering, Nagoya University, Furo-cho, Chikusa-ku, Nagoya, Aichi 464-8603, Japan

‡ PRESTO, Japan Science and Technology Agency (JST), Kawaguchi, Saitama 332-0012, Japan

Dedicated to Professor Shigeru Yamago on the occasion of his 60th birthday

Supporting Information Placeholder

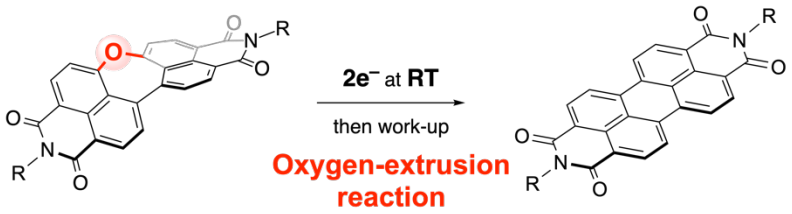

The synthesis and properties of a dinaphthooxepine bisimide (DNOBI), a non-planar perylene bisimide (PBI) analogue with an inserted oxygen atom, are described. A DNOBI underwent an oxygen-extrusion reaction smoothly upon electron injection at room temperature, affording PBI in good yield.

ABSTRACT: We report the synthesis and properties of a dinaphthooxepine bisimide (DNOBI), a non-planar perylene bisimide (PBI) analogue with an inserted oxygen atom. A DNOBI underwent an oxygen-extrusion reaction smoothly upon electron injection at room temperature, affording PBI in good yield. Studies on the reaction mechanism suggest that the injection of two electrons triggers the isomerization of DNOBI to dinaphthooxanorcaradiene bisimide, which is a key step in inducing the oxygen-extrusion reaction.

Non-planar π-systems exhibit various intriguing properties, such as three-dimensional conformations, structural flexibility, high solubility, and chirality.[1] Furthermore, several non-planar π-systems exhibit interesting reactivity because their significant structural distortion leads to the accumulation of molecular strain.[2–6] Representative examples are (1) the inner-selective functionalization of bowl-shaped aromatic hydrocarbons,[2] (2) the C–C-bond activation of cyclic nanocarbons,[3] (3) the reversible σ-bond formation of curved π-radicals,[4] and (4) sulfur- and phosphorus-extrusion reactions from a distorted seven-membered ring.[5,6]

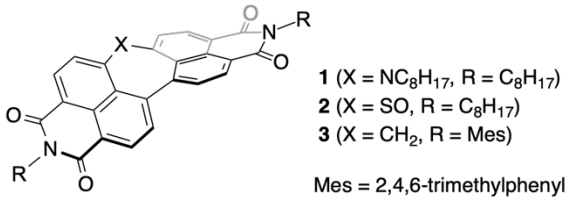

Figure 1. Element-inserted PBIs **1**–**3**.

Our group has recently developed a new family of non-planar π-systems, namely, element-inserted perylene bisimides (PBIs) including dinaphthoazepine bisimide (DNABI) **1**, dinaphthothiepine bisimide (DNTBI) *S*-oxide **2**, and dinaphthocycloheptatriene bisimide (DNCHepBI) **3**. (Figure 1).[7–10] These molecules exhibited unique stimulus-responsiveness and reactivity. Notably, dinaphthothiepine bisimide (DNTBI) *S*-oxide **2**, a sulfur-inserted PBI derivative, undergoes a sulfur-extrusion reaction upon heating, photo-irradiation, and electron injection, which enables the fabrication of n-type organic field-effect transistors by a solution process.[8]

Herein, we describe the synthesis and properties of dinaphthooxepine bisimides (DNOBIs) **4a** and **4b**, which represent oxygen-inserted PBI derivatives. Although the synthesis of dinaphthooxepine has been demonstrated by König and co-workers in 2014,[11] its imide-functionalized derivatives have not yet been reported to the best of our knowledge. Notably, a DNOBI underwent an oxygen-extrusion reaction smoothly upon electron injection at room temperature, affording PBI. This transformation is crucially different from the stepwise conversion of oxepine to benzene, which proceeds via (1) the thermal isomerization of oxepine to oxanorcaradiene, (2) the hydrogenation of an epoxide unit with $LiAlH_4$, and (3) dehydration.[12] While various organosulfur compounds are susceptible to sulfur extrusion reactions,[5,13] oxygen extrusion reactions[14–16] are rare because of the high bond energy of $C(sp^2)$–O bonds and the low Lewis basicity of the oxygen atom. Conventional strategies for transforming ethereal C–O bonds often require (a) harsh reductive conditions ($NaOtBu/LiAlH_4$ at 180 °C; Na in liq. NH_3),[14] (b) photo-irradiation,[15] or (c) the aid of transition metals at high temperatures.[16]

The synthesis of DNOBIs **4a** and **4b** is shown in Scheme 1. Initially, 5,5′-linked 4-chloro-1,8-naphthalic anhydride dimer[9] **5** was treated with 2,4,6-trimethylaniline and 2,2,3,3,4,4,4-heptafluorobutylamine to provide the corresponding imides **6a** and **6b** in 81 and 95% yield, respectively. Treatment of **6a** and **6b** with α-benzaldoxime in the presence of sodium hydride[17] induced double substitution at the chlorinated carbons with an oxygen atom, affording DNOBI **4a** and **4b** in 22% and 11% yield, respectively.

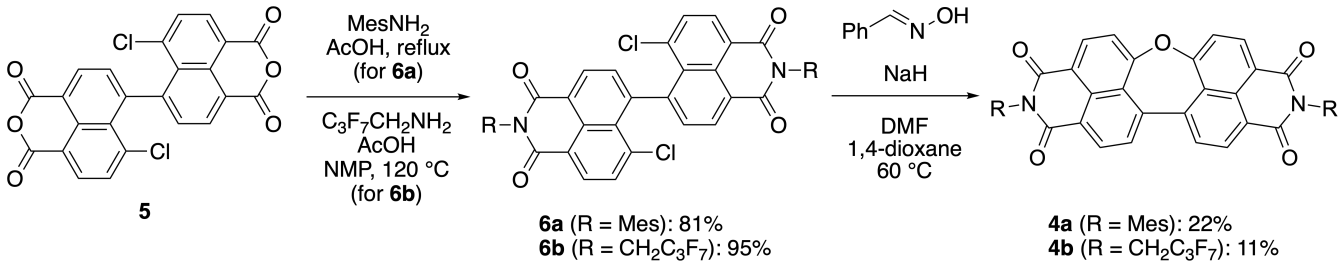

Scheme 1. Synthesis of DNOBIs **4a** and **4b.**

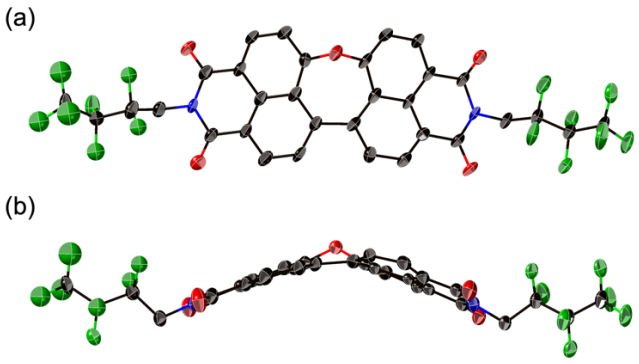

Figure 2. X-ray crystal structure of **4b** with thermal ellipsoids at 50% probability; (a) top and (b) side views; all hydrogen atoms are omitted for clarity (color code: grey = carbon; blue = nitrogen; red = oxygen; green = fluorine).

The solid-state structure of DNOBI **4b** was unambiguously determined by single-crystal X-ray diffraction analysis (Figure 2). DNOBI **4b** adopts a bent structure in which the central oxygen unit protrudes from the π-surface. This structure resembles that of dinaphthooxepine.[11] The length of the C–O bonds (1.392(6)/1.395(5) Å) is comparable to that of C–O bonds in diphenyl ether (1.381(2)/1.392(2) Å)[18] and dinaphthooxepine (1.380(2)/1.384(2) Å).[11] The structure of DNOBI was simulated using density functional theory (DFT) calculations at the B3LYP/6-31G(d) level, in which the imide substituents were replaced with methyl groups to simplify the calculations. Although the experimentally determined crystal structure was used as the initial structure, the optimization afforded a twisted structure without protrusion of the central oxygen (Figure S32). In the crystal packing of **4b**, the bent molecules stack in alternating directions to form a one-dimensional array (Figure S31), which should be the reason why **4b** adopts an inherently unfavorable bent structure in the solid state.

The UV/vis absorption and emission spectra of DNOBI **4a** are shown in Figure 3. DNOBI **4a** exhibits broad absorption at 300–500 nm with the peak top at 400 nm, which is hypsochromically shifted relative to that of PBI (up to 550 nm). These spectral features are characteristic of element-inserted PBIs.[7-10] The absorption of **4a** is also hypsochromically shifted compared to that of nitrogen-inserted PBI analogue **1** (up to 550 nm),[7] which can be attributed to the less effective electron-donating ability of an oxygen atom relative to that of a nitrogen atom. Time-dependent DFT (TD-DFT) calculations for **4a** suggested that (1) the [HOMO]–[LUMO] transition is forbidden (oscillator strength: 0.003), and that (2) the absorption at 300–500 nm is due to a combination of the [HOMO–1]–[LUMO] and [HOMO]–[LUMO+1] transitions (oscillator strength: 0.734) (Figure S33). These spectral features originate from the distribution of orbitals; the HOMO and LUMO+1 exhibit large orbital coefficients around the electron-donating oxygen atom, while the LUMO and HOMO–1 are mainly distributed over the opposite side of the oxygen atom (Figure S32). The emission spectrum of DNOBI **4a** is observed at 450–650 nm with peak tops at 484 and 508 nm (Figure 3). The emission quantum yield, Φ_F, and lifetime, τ, of **4a** are 30% and 2.9 ns, respectively. These parameters furnish radiative and non-radiative decay rate constants of 1.1×10^8 s^{-1} and 2.4×10^8 s^{-1}, respectively.

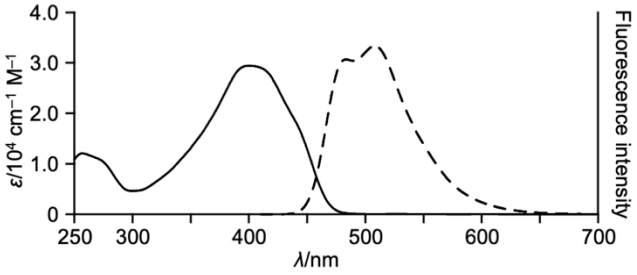

Figure 3. UV/vis absorption (solid lines) and emission (dashed lines) spectra of **4a** in CH_2Cl_2; λ = wavelength; ε = extinction coefficient.

The cyclic voltammogram of **4a** was measured in CH_2Cl_2 using the ferrocene/ferrocenium couple (Fc/Fc^+) as an external reference (Figures 4). Upon sweeping from –0.1 V to –1.5 V, DNOBI **4a** exhibits a peak at –1.26 V due to the electrochemical reduction in the first cycle (red). Interestingly, the subsequent backsweep affords peaks at –1.02 V and –0.82 V, which cannot be accounted for by the simple reoxidation of the *in-situ*-generated electron-injected species of **4a**. Moreover, the second cycle (blue) affords a different voltammogram, which is identical to that of PBI **7** (Figure S36). These results suggest that **4a** undergoes an oxygen-extrusion reaction upon electron injection. It is worth noting that previously reported dinaphthooxepine exhibited a reversible reduction wave, which indicates that the peripheral imide substituents are indispensable for the oxygen extrusion reaction.[11] Furthermore, DNABI **1**, a nitrogen-inserted PBI derivative, also exhibited a reversible reduction wave, indicating that **1** does not undergo a nitrogen-extrusion reaction upon electron injection.

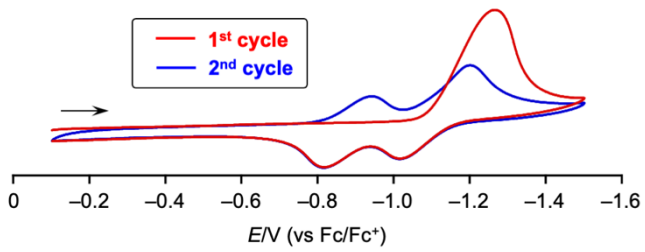

Figure 4. Cyclic voltammogram of **4a**.

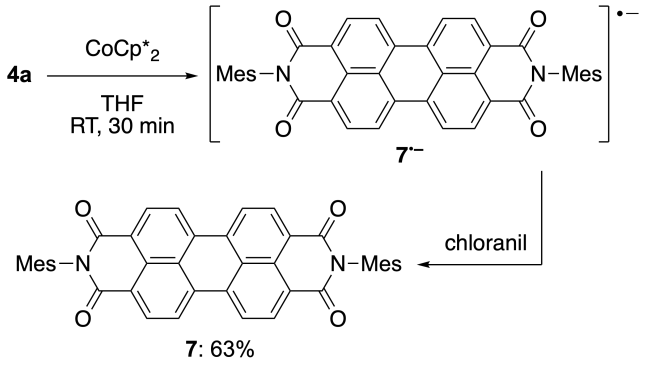

Scheme 2. Oxygen-extrusion reaction of **4a.**

To confirm the generation of PBI **7** upon electron injection, we examined the chemical transformation of **4a** (Scheme 2). For that purpose, 2.0 equiv. of decamethylcobaltocene ($CoCp^*_2$) was added at room temperature to a solution of **4a** in THF. The color of the solution immediately changed from light yellow to deep blue due to the generation of PBI radical anion $\mathbf{7}^{\bullet-}$, which was confirmed using titration experiments (*vide infra*). The mixture was stirred at room temperature for 30 min. The generated radical anion $\mathbf{7}^{\bullet-}$ was oxidized with chloranil to afford PBI **7** in 63% yield after purification. Reducing the amount of $CoCp^*_2$ to 1.0 equiv resulted in the recovery of **4a** (71%) along with a small amount of **7** (15%), as determined from the ^{1}H NMR analysis of the crude mixture. We also examined the use of KI-supported potassium metal and potassium graphite instead of $CoCp^*_2$ in the presence of [2.2.2]cryptand. Both reagents also induced the oxygen-extrusion reaction, suggesting that the counterion of the electron-injected DNOBI does not play a crucial role in removing the oxygen atom. It is worth noting that **4a** does not undergo oxygen-extrusion reactions upon photo-irradiation or heating, unlike sulfur-inserted PBI **2a**.[8]

We monitored the changes in the absorption spectra of **4a** upon adding $CoCp^*_2$ (Figure 5). These experiments were conducted under an argon atmosphere in degassed THF. Upon adding 1.0 equiv of $CoCp^*_2$, new absorption bands appeared in the 450–1400 nm region, and the absorption due to **4a** decreased (Figure 5a). The spectral pattern in the 450–1000 nm region is identical to that of PBI radical anion $\mathbf{7}^{\bullet-}$ (Figure S37). TD-DFT calculations suggested that the broad absorption at 1000–1400 nm is due to DNOBI radical anion $\mathbf{4a}^{\bullet-}$ (Figure S34). The further addition of $CoCp^*_2$ resulted in the following spectral changes: (1) a decrease in the absorption due to **4a** at 330–450nm, (2) an increase in the absorption due to PBI radical anion $\mathbf{7}^{\bullet-}$ at 450–1000 nm, and (3) a decrease in the broad absorption band due to at DNOBI radical anion $\mathbf{4a}^{\bullet-}$ at 1000–1400 nm. These results suggest that the oxygen-extrusion reaction proceeds after the generation of dianion $\mathbf{4a}^{2-}$.

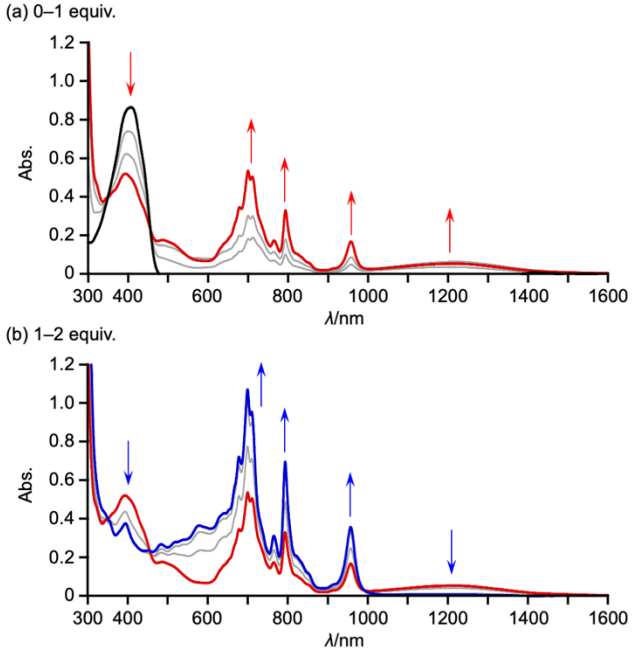

Figure 5. Changes in the UV/vis absorption spectra of **4a** upon adding $CoCp^*_2$ in THF under an argon atmosphere; $[\mathbf{4a}]_0 = 3.3 \times 10^{-5}$ M^{-1}; inset: absorption spectrum of PBI radical anion $\mathbf{7}^{\bullet-}$ in THF.

The structure and conformational dynamics of the dianion intermediate were studied by DFT calculations at the B3LYP/6-31G(d) level using the *Gaussian 16* software package and the global reaction route mapping (GRRM17)[19] program (Figure 6). To reduce the calculation costs, *N*-methyl-derivative $\mathbf{4c}^{2-}$ was used in these calculations. The solvent effect of THF was considered using the polarizable continuum model (PCM). Two initial geometries were employed to obtain the optimized structure of dianion $\mathbf{4c}^{2-}$, i.e., (1) a bent structure identical to the crystal structure of **4b** and (2) the twisted structure produced by the DFT optimization of neutral DNOBI **4c**. However, the structural optimization afforded the same bent structure in both cases, in which the distance between the oxygen-substituted carbons is 2.315 Å. The structural change of dianion $\mathbf{4c}^{2-}$ was simulated and revealed that $\mathbf{4c}^{2-}$ isomerizes to dinaphthooxanorcaradiene bisimide $\mathbf{8c}^{2-}$ with a shortened C–C distance of 1.509 Å. The activation energy was calculated to be 13.3 kcal mol^{-1}, which indicates that this isomerization proceeds even at room temperature.

The exact reaction pathway to PBI radical anion $\mathbf{7}^{\bullet-}$ after the generation of $\mathbf{8c}^{2-}$ is not clear at this moment. The simplest scenario could be: (1) protonation of the oxygen atom of $\mathbf{13c}^{2-}$, followed by (2) elimination of a hydroxy radical. However, coumarin, which is a typical hydroxy radical scavenger,[20] remained intact after the reaction of **4a** with $CoCp^*_2$ in THF.

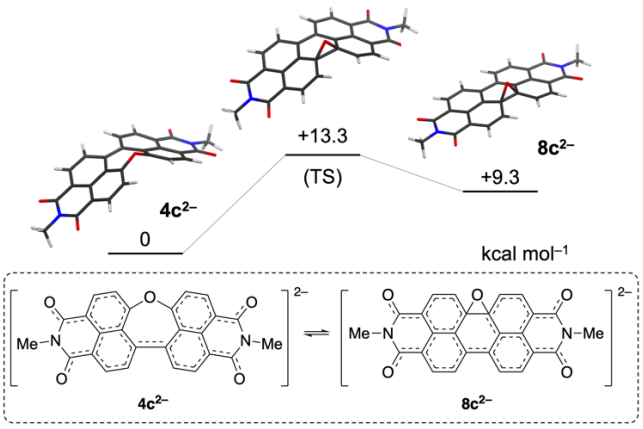

Figure 6. Simulated isomerization pathway of dianion $\mathbf{4c}^{2-}$. The calculations were conducted at the B3LYP/6-31G(d) level. The solvent effect (THF) was accounted for using the polarizable continuum model (PCM).

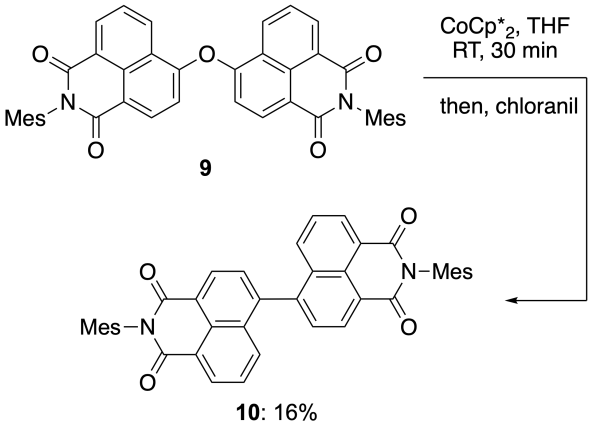

Scheme 3. Oxygen-extrusion reaction of **9.**

To explore the role of an embedded seven-membered ring, we synthesized oxygen-bridged naphthalene monoimide (NMI) dimer **9** (Scheme S1). Treatment of **9** with $CoCp^*_2$ also induced oxygen extrusion to yield 4–4′ linked NMI dimer **10**, albeit that the crude mixture was relatively messy compared to that of **4a**, resulting in a low yield of **10** (16%) (Scheme 3). Other side products were difficult to isolate due to the trace amount. This result indicates that the presence of an oxepine subunit in **4a** is not essential to realize the observed oxygen-extrusion reaction. It is likely that the structural confinement in **4a** due to the C–C bond between the two NMI units suppresses undesirable side reactions.

In summary, we have synthesized dinaphthooxepine bisimides (DNOBIs) **4a** and **4b**. Their molecular design is based on the insertion of an oxygen atom into a perylene bisimide (PBI) core. DNOBI **4a** undergoes oxygen extrusion upon electron injection. Investigation for the reaction mechanism revealed that the injection of two electrons triggers the isomerization of DNOBI to dinaphthooxanorcaradiene bisimide, which is a key step in inducing the oxygen-extrusion reaction. Moreover, we prepared oxygen-bridged naphthalene monoimide dimer **9**, which also undergoes an oxygen-extrusion reaction upon electron injection. The current results offer a new entry in the interesting reactivity of non-planar π-systems. Furthermore, considering that carbon(sp^2)–oxygen bonds are found in many biological or artificial materials, such as lignin and poly(ether-ether-ketone), this study thus offers fundamental insight into the development of rational strategies to cleave ethereal C–O bonds, which are abundant in biomass and plastics.

ASSOCIATED CONTENT

Data Availability Statement

The data underlying this study are available in the published article and its Supporting Information.

Supporting Information Statement

The Supporting Information is available free of charge on the ACS Publications website.
Experimental details and spectral data for all new compounds.
Crystallographic data (CIF file) for **4b**.

AUTHOR INFORMATION

Corresponding Author

fukui@chembio.nagoya-u.ac.jp, hshino@chembio.nagoya-u.ac.jp

ACKNOWLEDGMENT

This work was supported by JSPS KAKENHI grants JP20H05862 (H.S., N.F.), JP20H05863 (H.S.), JP20K15257 (N.F.), JP20H05867 (N.F.), and JP22K14663 (N.F.), as well as by JST, PRESTO grant JPMJPR21Q7 (N.F.). The authors thank Prof. Makoto Yamashita, Mr. Masahiro Yamamoto, and Mr. Yoshiki Sugano (Nagoya University) for fruitful discussions and support with the experiments involving potassium.

REFERENCES

(1) (a) Gingras, M. One Hundred Years of Helicene Chemistry. Part 3: Applications and Properties of Carbohelicenes. *Chem. Soc. Rev.* **2013**, *42*, 1051–1095. (b) Kawase, T.; Kurata, H. Ball-, Bowl-, and Belt-Shaped Conjugated Systems and Their Complexing Abilities: Exploration of the Concave−Convex π-π Interaction. *Chem. Rev.* **2006**, *106*, 5250–5273. (c) Qu, Y.-T.; Siegel, J. S. Aromatic Molecular-Bowl Hydrocarbons: Synthetic Derivatives, Their Structures, and Physical Properties. *Chem. Rev.* **2006**, *106*, 4843–4867. (d) Pascal, R. A. Twisted Acenes. *Chem. Rev.* **2006**, *106*, 4809–4819. (e) Shen, Y.; Chen, C.-F. Helicenes: Synthesis and Applications. *Chem. Rev.* **2012**, *112*, 1463–1535. (f) Bodwell, G. J. Extraordinary Transformations to Achieve the Synthesis of Remarkable Aromatic Compounds. *Chem. Rec.* **2014**, *14*, 547–567. (g) Segawa, Y.; Yagi, A.; Matsui, K.; Itami, K. Design and Synthesis of Carbon Nanotube Segments. *Angew. Chem., Int. Ed.* **2016**, *55*, 5136–5138. (h) Satoru, H. Innovative Synthesis and Functions of Curved π-Conjugated Molecules. *Bull. Chem. Soc. Jpn.* **2018**, *91*, 829–838. (i) Saito, M.; Shinokubo, H.; Sakurai, H. Figuration of Bowl-Shaped π-Conjugated Molecules: Properties and Functions *Mater. Chem. Front.* **2018**, *2*, 635–661. (j) Márquez, I. R.; Castro-Fernández, S.; Millán, A.; Campaña, A. Synthesis of distorted nanographenes containing seven- and eight-membered carbocycles. *Chem. Commun.* **2018**, *54*, 6705–6718. (k) Majewski, M. A.; Stępień, M. Bowls, Hoops, and Saddles: Synthetic Approaches to Curved Aromatic Molecules. *Angew. Chem., Int. Ed.* **2019**, *58*, 86–116.

(2) (a) Fernández, I. Understanding the reactivity of polycyclic aromatic hydrocarbons and related compounds. *Chem. Sci.* **2020**, *11*, 3769–3779. (b) Preda, D. V.; Scott, L. T. Addition of Dihalocarbenes to Corannulene. A Fullerene-Type Reaction. *Tetrahedron Lett.* **2000**, *41*, 9633–9637. (c) Cho, H. Y.; Ansems, R. B. M.; Scott, L. T. Site-Selective Covalent Functionalization at Interior Carbon Atoms and on the Rim of Circumtrindene, a $C_{36}H_{12}$ Open Geodesic Polyarene. *Beilstein J. Org. Chem.* **2014**, *10*, 956–958. (d) Zabula, A. V.; Spisak, S. N.; Filatov, A. S.; Rogachev, A. Y.; Petrukhina, M. A. A Strain-Releasing Trap for Highly Reactive Electrophiles: Structural Characterization of Bowl-Shaped Arenium Carbocations. *Angew. Chem., Int. Ed.* **2011**, *50*, 2971–2974. (e)

Ngamsomprasert, N.; Dang, J.-S.; Higashibayashi, S.; Yakiyama, Y.; Sakurai, H. Sumanene Derivatives Functionalized at the Internal Carbon. *Chem. Commun.* **2017**, *53*, 697–700. (f) Bronstein, H. E.; Scott, L. T. Fullerene-like Chemistry at the Interior Carbon Atoms of an Alkene-Centered $C_{26}H_{12}$ Geodesic Polyarene. *J. Org. Chem.* **2008**, *73*, 88–93. (g) Yanney, M.; Fronczek, F. R.; Sygula, A. Corannulene Subunit Acts as a Diene in a Cycloaddition Reaction: Synthesis of $C_{80}H_{32}$ Corannulyne Tetramer. *Org. Lett.* **2012**, *14*, 4942–4945. (h) Dubceac, C.; Zabula, A. V.; Filatov, A. S.; Rossi, F.; Zanello, P.; Petrukhina, M. A. Bowl-Shaped Carbocations: Easy to Produce, Hard to Reduce. *J. Phys. Org. Chem.* **2012**, *25*, 553–558.

(3) (a) Kayahara, E.; Hayashi, T.; Takeuchi, K.; Ozawa, F.; Ashida, K.; Ogoshi, S.; Yamago, S. Strain-Induced Double Carbon–Carbon Bond Activations of Cycloparaphenylenes by a Platinum Complex: Application to the Synthesis of Cyclic Diketones. *Angew. Chem., Int. Ed.* **2018**, *57*, 11418–11421. (b) Kurosaki, R.; Hayashi, H.; Suzuki, M.; Jiang, J.; Hatanaka, M.; Aratani, N.; Yamada, H. A Remarkably Strained Cyclopyrenylene Trimer that Undergoes Metal-Free Direct Oxygen Insertion into the Biaryl C–C σ-Bond. *Chem. Sci.* **2019**, *10*, 6785–6790.

(4) Yokoi, H.; Hiroto, S.; Shinokubo, H. Reversible σ-Bond Formation in Bowl-Shaped π-Radical Cations: The Effects of Curved and Planar Structures. *J. Am. Chem. Soc.* **2018**, *140*, 4649–4655.

(5) (a) Hoffman Jr., J. M.; Schlessinger, R. H. Synthesis of a Stable 8-π-Electron Thiepin. *J. Am. Chem. Soc.* **1970**, *92*, 5263–5265. (b) Nishino, K.; Yano, S.; Kohashi, Y.; Yamamoto, K.; Murata, I. Synthesis of 2,7-Di-*tert*-butyl-4-ethoxycarbonyl-5-methylthiepin. A Remarkably Stable and Simple Monocyclic Thiepin. *J. Am. Chem. Soc.* **1979**, *101*, 5059–5060. (c) Gleiter, R.; Krennrich, G.; Cremer, D.; Yamamoto, K.; Murata, I. Electronic Structure and Thermal Stability of Thiepins. Photoelectron Spectroscopic Investigations. *J. Am. Chem. Soc.* **1985**, *107*, 6874–6879.

(6) Borst, M. L. G.; Bulo, R. E.; Winkel, C. W.; Gibney, D. J.; Ehlers, A. W.; Schakel, M.; Lutz, M.; Spek, A. L.; Lammertsma, K. Phosphepines: Convenient Access to Phosphinidene Complexes. *J. Am. Chem. Soc.* **2005**, *127*, 5800–5801.

(7) Hayakawa, S.; Kawasaki, A.; Hong, Y.; Uraguchi, D.; Ooi, T.; Kim, D.; Akutagawa, T.; Fukui, N.; Shinokubo, H. Inserting Nitrogen: An Effective Concept To Create Nonplanar and Stimuli-Responsive Perylene Bisimide Analogues. *J. Am. Chem. Soc.* **2019**, *141*, 19807–19816.

(8) Hayakawa, S.; Matsuo, K.; Yamada, H.; Fukui, N.; Shinokubo, H. Dinaphthothiepine Bisimide and Its Sulfoxide: Soluble Precursors for Perylene Bisimide. *J. Am. Chem. Soc.* **2020**, *142*, 11663–11668.

(9) Tanaka, Y.; Tajima, K.; Fukui, N.; Shinokubo, H. Dinaphtho[1,8-*bc*:1′,8′-*fg*][1,5]dithiocine Bisimide. *Asian J. Org. Chem.* **2021**, *10*, 541–544.

(10) Odajima, M.; Tajima, K.; Fukui, N.; Shinokubo, H. Non-Planar Perylene Bisimide Analogues with Inserted Carbonyl and Methylene Subunits. *Angew. Chem., Int. Ed.* **2021**, *60*, 15838–15843.

(11) Dobelmann, L.; Parham, A. H.; Büsing, A.; Buchholz, H.; König, B. First synthesis of naphthalene annulated oxepins. *RSC Adv.* **2014**, *4*, 60473–60477.

(12) Vogel, E.; Günther, H. Benzene Oxide-Oxepin Valence Tautomerism. *Angew. Chem., Int. Ed.* **1967**, *6*, 385–476.

(13) (a) Taylor, R. J. Recent developments in Ramberg–Bäcklund and episulfone chemistry. *Chem. Commun.* **1999**, 217–227. (b) Boekelheide, V.; Reingold, I. D.; Tuttle, M. Syntheses of cyclophanes by photochemical extrusion of sulphur. *J. Chem. Soc. Chem. Commun.* **1973**, 406–407. (c) Armarego, W. L. F. 83. The synthesis of two dinaphthothiophens. *J. Chem. Soc.* **1960**, 433–436. (d) Schroth, W.; Hintzsche, E.; Felicetti, M.; Spitzner, R.; Sieler, J.; Kempe, R. Concerning the Questionable Existence of Thioxoindigoid Compounds. *Angew. Chem., Int. Ed. Engl.* **1994**, *33*, 739–741. (e) Wakamiya, A.; Nishinaga, T.; Komatsu, K. Generation and oligomerization of bicyclo[2.2.2]octyne and properties of tris(bicyclo[2.2.2]octeno)benzene obtained from the linear trimer. *J. Am. Chem. Soc.* **2002**, *124*, 15038–15050. (f) Kamiya, H.; Kondo, T.; Sakida, T.; Yamaguchi, S.; Shinokubo, H. *meso*-Thiaporphyrinoids Revisited: Missing of Sulfur by Small Metals. *Chem.-Eur. J.* **2012**, *18*, 16129–16135. (g) Christensen, P. R.; Patrick, B. O.; Caron, É.; Wolf, M. O. Oxidation-State-Dependent Photochemistry of Sulfur-Bridged Anthracenes. *Angew. Chem., Int. Ed.* **2013**, *52*, 12946–12950. (h) Murata, M.; Maeda, S.; Morinaka, Y.; Murata, Y.; Komatsu, K. Synthesis and Reaction of Fullerene C_{70} Encapsulating Two Molecules of H_2. *J. Am. Chem. Soc.* **2008**, *130*, 15800–15801.

(14) (a) Xu, H.; Yu, B.; Zhang, H.; Zhao, Y.; Yang, Z.; Xu, J.; Han, B.; Liu, Z. Reductive Cleavage of Inert Aryl C–O Bonds to Produce Arenes. *Chem. Commun.* **2015**, *51*, 12212–12215. (b) Strojny, E. J. Cleavage of *o*- and *p*-Biphenylyl Phenyl Ethers with Sodium and Liquid Ammonia. *J. Org. Chem.* **1966**, *35*, 1662.

(15) Haga, N.; Takayanagi, H. Mechanisms of the Photochemical Rearrangement of Diphenyl Ethers. *J. Org. Chem.* **1996**, *61*, 735–745.

(16) (a) Yu, D.-G.; Li, B.-J.; Shi, Z.-J. Exploration of New C–O Electrophiles in Cross-Coupling Reactions. *Acc. Chem. Res.* **2010**, *43*, 1486–1495. (b) Cornella, J.; Zarate, C.; Martin, R. Metal-Catalyzed Activation of Ethers via C–O Bond Cleavage: A New Strategy for Molecular Diversity. *Chem. Soc. Rev.* **2014**, *43*, 8081–8097. (c) Tobisu, M.; Chatani, N. Nickel-Catalyzed Cross-Coupling Reactions of Unreactive Phenolic Electrophiles via C–O Bond Activation. *Top. Curr. Chem.* **2016**, *374*, 41. (d) Wenkert, E.; Michelotti, E. L.; Swindell, C. S. Nickel-Induced Conversion of Carbon-Oxygen into Carbon-Carbon Bonds. One-step Transformations of Enol Ethers into Olefins and Aryl Ethers into Biaryls. *J. Am. Chem. Soc.* **1979**, *101*, 2246–2247.

(17) Nishiyama, A.; Fukuda, M.; Mori, S.; Furukawa, K.; Fliegl, H.; Furuta, H.; Shimizu, S. Rational Synthesis of Antiaromatic 5,15-Dioxaporphyrin and Oxidation into *β*,*β*-Linked Dimers. *Angew. Chem., Int. Ed.* **2018**, *57*, 9728–9733.

(18) Choudhury, A. R.; Islam, K.; Kirchner, M. T.; Mehta, G.; Row, T. N. G. In Situ Cryocrystallization of Diphenyl Ether: C—H···π Mediated Polymorphic Forms. *J. Am. Chem. Soc.* **2004**, *126*, 12274–12275.

(19) Maeda, S.; Harabuchi, Y.; Takagi, M.; Saita, K.; Suzuki, K.; Ichino, T.; Sumiya, Y.; Sugiyama, K.; Ono, Y. Implementation and Performance of the Artificial Force Induced Reaction Method in the GRRM17 Program. *J. Comp. Chem.* **2018**, *39*, 233–251.

(20) Maier, A. C.; Iglebaek, E. H.; Jonsson, M. Confirming the Formation of Hydroxyl Radicals in the Catalytic Decomposition of H_2O_2 on Metal Oxides Using Coumarin as a Probe. *ChemCatChem* **2019**, *11*, 5435–5438.